Landau level anticrossing manifestations in the phase-diagram topology of a two-subband system

X. C. Zhang,[1] I. Martin,[2] and H. W. Jiang[1]

[1]*Department of Physics and Astronomy, University of California at Los Angeles,*
405 Hilgard Avenue, Los Angeles, California 90095, USA
[2]*Theoretical Division, Los Alamos National Laboratory, Los Alamos, New Mexico 87545, USA*

In a two-subband GaAs/AlGaAs two-dimensional electron system, the phase diagram of longitudinal resistivity ρ_{xx} in density and magnetic field plane exhibits an intriguing structure centered at filling factor $\nu=4$ which is strikingly different from the ringlike structures at lower magnetic fields. Thermal activation measurements reveal an anticrossing gap on each boundary of the structure where intersubband Landau levels with parallel or antiparallel spin are brought into degeneracy. While the physics of the anticrossing can be ascribed to the pseudospin quantum Hall ferromagnetism, as reported earlier by Muraki *et al.*, the mapping and modeling of the phase-diagram topology allow us to establish a more complete picture of the consequences of real spin/pseudospin interactions for the two-subband system.

A two-subband electron system, which can be either a wide single quantum well or a coupled double quantum well, becomes particularly appealing for studying correlation effects when the two sets of Landau levels (LLs) are brought into degeneracy by varying magnetic field or carrier concentration.[1] The correlation effects can be intriguing near these degeneracy points, since in addition to the interaction of the real electron spins, there is also a strong correlation of the two subband charge states, referred to in the literature as pseudospins.[2–6] For example, in an earlier study it was found that the experimentally determined phase diagram of a single well two-subband system, exhibits "ringlike structures" at even integer filling factors[7] near degeneracy points. Inside the rings, due to the exchange interactions of real spins, the electron spins of different subbands are aligned by the external magnetic field over an extended range of magnetic field and density.[8,9] On the other hand, an early work in a wider single well two-subband system, energy gaps were observed near the degeneracy points at filling factors of both $\nu=3$ and 4 (Ref. 10) which were interpreted as a result of the easy-plane or easy-axis quantum Hall ferromagnetism of the pseudospin charge states.

Here, we extend the study of the phase-diagram topology to higher magnetic fields up to 10 T, with the main objective to explore the interplay between the real spin and the pseudospin correlations. We found that the "ringlike" structures at low magnetic fields, centered around $\nu=6$, 8, 10, evolve into a "squarelike" structure at filling factor $\nu=4$ at higher magnetic fields which shows clear evidence of level anticrossing at its four boundaries. The evidence was established by both thermal activation gap measurement in the proximity of the expected LL degeneracy points, and also by reproducing key features in the phase-diagram topology using simulation of the density of states (DOS) of the anticrossed LLs. We believe the anticrossings exhibited in our phase diagram are consistent with the early reported quantum Hall ferromagnetism of pseudospins.[10]

The sample used in this work is a symmetrical modulation-doped single quantum well with an equally 240 Å thick well and spacer. The sample details can be found in Ref. 7. At zero gate voltage the total electron den-

sity is 8.1×10^{11} cm^{-2}, the density in the ground and first excited subband are 5.4×10^{11} cm^{-2}, and 2.7×10^{11} cm^{-2}, respectively. The mobility is about 4×10^5 cm^2/V.s. The spin splitting is well resolved above 1.8 tesla for both subbands. The band edge profile and subband wave function envelopes are depicted in Fig. 1(b). A 100 μm wide Hall bar with 270 μm between voltage probes was patterned by standard lithography techniques. A NiCr top gate was used to vary the electron density. Measurements were made in a dilution refrigerator with a base temperature of 60 mK and in a perpendicular magnetic field normal to sample plane using ac lock-in techniques with a bias current of 10 nA.

The phase diagram, i.e., the plot of longitudinal resistivity ρ_{xx} as a function of magnetic field B and gate voltage V_g, is shown in Fig. 1(a). The most pronounced feature in this diagram is the last "squarelike structure" enclosed in the dashed line box, strikingly different from the reported ringlike structures at low magnetic fields.[7] The most noticeable feature of the squarelike structure is the *disappearance* of the extended states on its four boundaries, marked by "A," "B," "C," and "D" in Fig. 1(a). These are the places where spin split LLs of different subbands cross each other. The evolution from a ring to a square can be partly seen from the gradual disappearance of the extended states at the lower branch of the ring indicated by the three arrows. The labeled filling factors are read from the quantized values in units of e^2/h in transverse conductivity $1/\rho_{xy}$ simultaneously measured with ρ_{xx}.

Since there seems to exist a gap manifested by the disappearance of the extended states on each boundary of the square structure, it is natural to obtain a measurement of the energy scale of the associated gap size there. In Fig. 2(b) we present the Arrehenius plots with $\log(\rho_{xx})$ as a function of inverse temperature $1/T$ for four data points A, B, C, D marked by dots in Fig. 2(a), which are the center of each boundary of the square structure. The Arrehenius plots all show clear temperature activation behavior $\rho_{xx} \propto \exp(-E_a/2T)$, and the obtained activation energies of E_a are 2.70, 2.88, 3.34, 2.86 K for A, B, C, and D, respectively. The evolution of the gaps at $\nu=3$ and 4 along the dashed line in Fig. 2(a) are shown in Fig. 2(c). Both curves indicate an
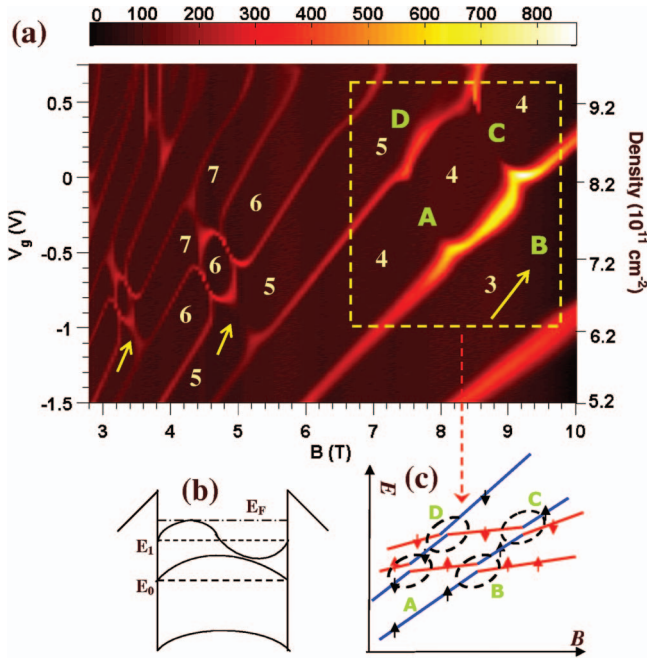
FIG. 1. (Color) (a), Plot of the longitudinal resistivity ρ_{xx} in the gate-voltage V_g and magnetic field B plane measured at 70 mK. The filling factors from ρ_{xy} measurement are labeled. A square structure at $\nu=4$ (inside the dashed line box) is observed at high magnetic fields, in contrast to the ring structures at low magnetic fields. (b) schematically shows band edge profile, energy quantization, and wave function envelope of our two-subband system. (c) depicts anticrossing occurred between spin split intersubband LLs on four corresponding places in (a) marked by A, B, C, and D.

anticrossing gap signified by a minimum at A and B, respectively. Apparently, the gap at $\nu=4$ undergoes a much more rapid transition as a function of magnetic field.

We believe the anticrossings, or energy gaps, observed here have the same origin as those reported earlier by Muraki *et al.* in a similar two-subband system.[10] The authors suggested that the minima in the activation energy are results of pseudospin quantum Hall ferromagnetism, which lifts the degeneracy near the Landau level crossing points. It has been recognized in recent years that when two Landau levels with different symmetry of their wave functions, labeled as pseudospin up and down states, simultaneously approach the chemical potential at integer filling factors,[2] the ferromagnetic state of the pseudospins becomes energetically favorable. The resultant pseudospin anisotropy energy depends on the details of both orbital and spin states of the LLs involved, accordingly the system can exhibit easy axis or easy plane anisotropy. The activation gap in the longitudinal resistivity corresponds to the energy required to create an unbound particle-hole excitation in such an insulating ferromagnetic state. Following the analysis of Ref. 10, the activation energy E_a is replotted versus the effective Zeeman energy ΔE_z in Fig. 3 for $\nu=4$ and 3, respectively, both normalized by characteristic Coulomb energy $e^2/4\pi\varepsilon\cdot l_B$, where $l_B=(\hbar/eB)^{1/2}$ is magnetic length. The single particle energy difference ΔE_z acts as an *effective* Zeeman energy,

$$\Delta E_z = \left(|\Delta N|\frac{\hbar e}{m^*} + \Delta\sigma|g|\mu_B\right) \times (B - B_C). \quad (1)$$

ΔN or $\Delta\sigma$ is the LL or spin index change at crossing field B_c. $\Delta N=1(1)$ and $\Delta\sigma=\pm 1(0)$ for LL crossing at $\nu=4(3)$.
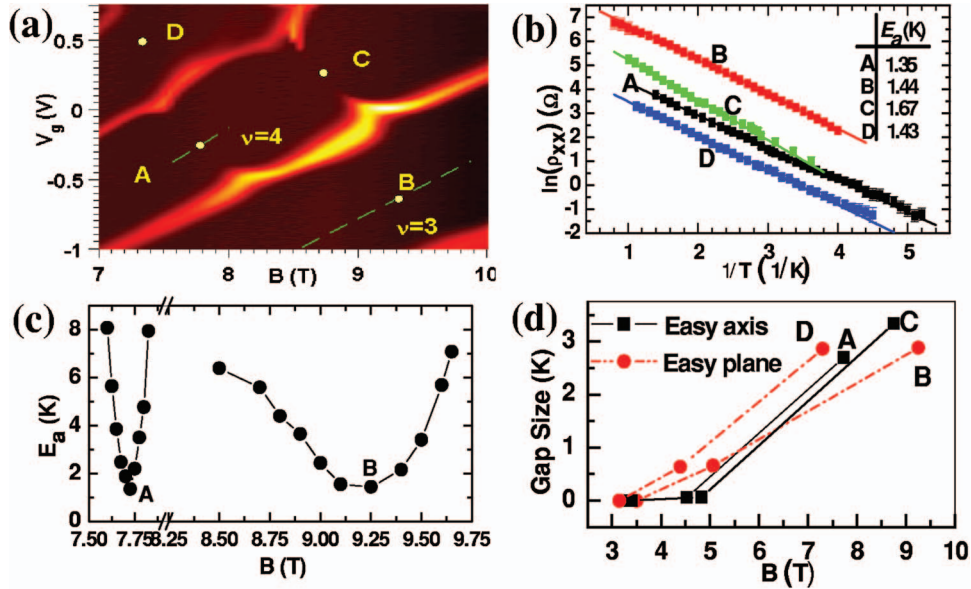

FIG. 2. (Color) (a), An enlarged view of the portion enclosed by box in Fig. 1(a). Yellow dots A($Vg=-0.207$ V/$B=7.725$ T), B(-0.62 V/9.25 T), C(0.241 V/8.75 T), and D(0.505 V/7.3 T) are roughly middle point of each boundary of the ring where LLs are crossed. (b), Arrhenius plots of log(ρ_{xx}) versus $1/T$ for points A, B, C, and D. The straight lines are linear regression of experimental data. The activation energies are displayed in the inset table. (c), Activation energy measured along the two dashed line centered at position A and B in (a) shows clearly anticrossing gap. (d), Anticrossing gap measured at positions A, B, C, D for square (or ring) structure centered at $\nu=4,6,8$ as a function of B.
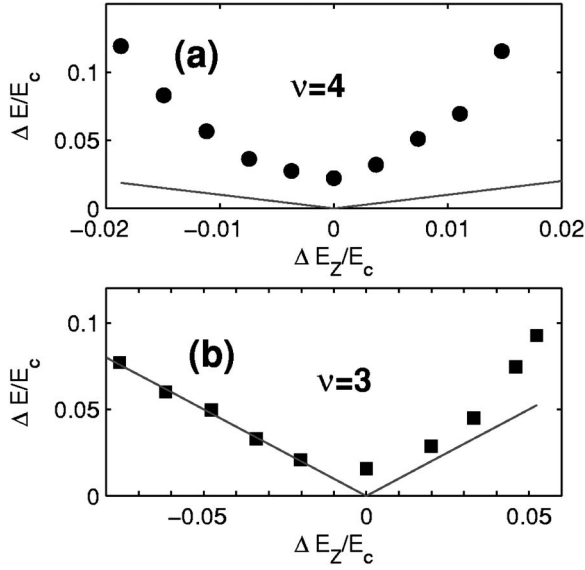
FIG. 3. Normalized experimental anticrossing gap ΔE (filled circles or squares) as a function of normalized single particle gap ΔE_z, both in units of $e^2/4\pi\varepsilon l_B$, where $l_B = (\frac{\hbar}{eB})^{1/2}$ is the magnetic length, at filling factor $\nu = 4$ (a) and $\nu = 3$ (b). The lines in each figure have a slope of 1 and denote the effective single particle gap along the two dashed line shown in Fig. 2(a).

$g = -0.44$ is the bare g factor. The gaps for $\nu = 3$ in Fig. 3(b) show a smooth transition whose asymptotes approach the single particle ΔE_z, indicated by the straight lines. This is consistent with a continuously evolving ground state which is a coherent superposition of two-subband pseudospins, or an easy-plane magnetization anisotropy.[2,10] The magnitudes of the gaps are consistent with the theoretical quasiparticle energy gap calculated by Jungwirth *et al.* for idealized easy-plane anisotropy.[3] On the contrary, normalized E_a at $\nu = 4$ in Fig. 3(a) shows a slope four times greater than the single particle Zeeman gap denoted by straight lines. This unusual behavior is likely to be caused by the easy-axis ferromagnetism. The high slope may be caused by the disorder-broadened gap hysteresis predicted by Jungwirth *et al.*[3] for the easy axis quantum Hall ferromagnets. While theory, predicts a first order transition between fully occupied subband levels in this case, a real system disorder will lead to finite-size domain formation, possibly softening the bulk transition to the second order, which is consistent with the smooth evolution of the activation gap in the vicinity of the $\nu = 4$ anticrossing. We note here that the slope enhancement that we observe is a factor of 10 smaller than in Muraki *et al.* which is likely caused by the difference in the system parameters, including the well width, carrier densities, and disorder.

It is instructive and interesting to check if we can understand the intriguing topological features of the phase diagram within the LL anticrossing picture. To that end we developed a simple analytical model based on DOS calculation of anticrossed spin split LLs with different subband indices. It turns out that by properly choosing the anticrossing gap, the main features of the phase diagram can be reproduced quite nicely. For a noninteracting two-subband system in a perpendicular magnetic field B, the energy spectrum is,
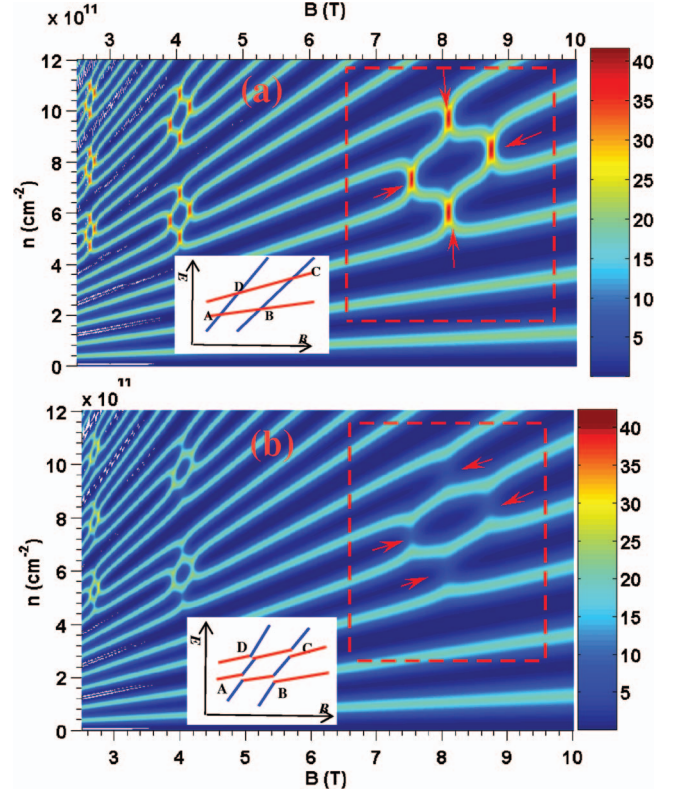

FIG. 4. (Color) Calculated resistivity (in arbitrary unit) topological diagram assuming zero anticrossing (a), and finite intersubband LL anticrossing gap $\Delta = 0.12$ meV at $B = 7.725$ T (b). The contrast between them is emphasized in the dashed box. Instead of a resistivity enhancement for zero anticrossing case, four clear gaps appear at the four boundaries of the last ring structure for finite anticrossing (indicated by arrows in boxes). The inset in each graph shows corresponding LL crossing (a) or anticrossing (b) situation in E-B plane.

$$E_{1,\pm} = \left(n + \tfrac{1}{2}\right)\hbar\omega_B \pm g^*\mu_B B, \tag{2a}$$

$$E_{2,\pm} = \left(n + \tfrac{1}{2}\right)\hbar\omega_B \pm g^*\mu_B B + \Delta E_{12}. \tag{2b}$$

$E_{1,\pm}$ and $E_{2,\pm}$ are energy of the ground and first excited state with different spin states, $\hbar\omega_B$ is the cyclotron energy, g^* is an electron effective g factor, μ_B is the Bohr magneton, ΔE_{12} is the energy offset between the two subbands. For level anticrossing, here we choose an energy dispersion of a generic square root form irrespective of the spin states,

$$E_A = \frac{(E_1 + E_2)}{2} + \sqrt{\frac{1}{4}(E_1 - E_2)^2 + \Delta^2}, \tag{3a}$$

$$E_B = \frac{(E_1 + E_2)}{2} - \sqrt{\frac{1}{4}(E_1 - E_2)^2 + \Delta^2}. \tag{3b}$$

E_A, E_B are antibonding and bonding states after level repulsion caused by anticrossing, E_1 and E_2 are single particle energy levels expressed by Eqs. (2a) and (2b). Δ is half of the anticrossing gap between two spin split LLs of different subbands. In order to directly compare with the experiment, we need to calculate the DOS of the anticrossed LLs. For

simplicity, we assume the resistivity, that is proportional to the DOS, takes a Lorentzian form. At a fixed magnetic field, for a certain electronic density n, the Fermi energy E_F can be determined by integrating the Lorentzian DOS over the occupied states ($E \lesssim E_F$) and making it equal to n. The DOS (i.e., the resistivity) can be deduced from this E_F. Repeating the procedure for different n and B, the whole topological phase diagram can be constructed as shown in Fig. 4 (Ref. 11). The top panel of Fig. 4(a) shows the result of zero anticrossing, i.e., the LLs just cross each other as in the normal case. The ring structures closely match the experimental diagram in Fig. 1(a) at low magnetic fields, which supports the validity of our model. As expected, because of the overlap of DOS, at each LL crossing point such as A, B, C, and D shown in the inset, the resistance value has a maximum marked by the arrows in the dashed line box. To account for the exchange interaction of the real spins, we have used an enhanced effective g-factor $g^* = -2.2$ for each subband, similar to that used by Ellenberger *et al.* recently.[12] It is apparent that this normal LL crossing picture fails completely to explain the conductance disappearance at the LL crossing points marked by A, B, C, D in Fig. 2(a). However, by using the experimental gap values (≈ 0.12 meV at 7.725 T) for Δ and assume it is a linear function of $B^{1/2}$ in Eq. (3), the squarelike structure readily comes out in high B as shown in Fig. 4(b). This exercise clearly indicates that the intersubband LL anticrossing effect is responsible for the "squarelike" structure in topological phase diagram.

Having mapped and modeled the phase-diagram topology, we may now gain some new insight for a better global understanding of the two-subband system. For example, it can be anticipated that along $\nu = 5$ an anticrossing should also occur which shares the same physics as $\nu = 3$ case. Second, the topological phase diagram in Fig. 1(a) displays an interesting interplay between the real spin and the pseudospin correlations as B increases. Along an even filling factor line sectioning through the ring (or square) structure, as shown in Fig. 2(a), it represents a paramagnetic to ferromagnetic phase transition induced by preferential alignment of *real* electron spins to save exchange energy in an external magnetic field.[7–9] At high B, *in addition*, the pseudospin correlation resultant easy-axis or easy-plane quantum Hall ferromagnetism at even or odd filling factors, respectively, opens up a gap at each boundary of the "ring" structure making it appear like a "square" at $\nu = 4$. Interestingly enough, the gap at odd filling factors appear to open up gradually with B evidenced by the gradual disappearance of the resistance at $\nu = 7$, 5, and 3 shown by the three arrows in Fig. 1(a). In contrast, the gap which occurred on the even filling factor boundary seems to open up suddenly at $\nu = 4$. The B dependence of the four anticrossing gaps around the square (or ring) structure at $\nu = 4$, 6, 8 is shown in Fig. 2(d). We speculate that the very different B dependence of the gaps at even and odd filling factors reflects the difference in the disorder effects in the easy-plane and easy-axis anisotropy cases. For instance, potential out-of-plane disorder can cause fluctuations in the position of the subband crossing point. While in the easy plane case, the electronic state can gradually adjust to such fluctuations via a smooth distortion, in the easy axis case, strong enough disorder fluctuations can make the structure with domains of fully occupied subband levels unsustainable, thus eliminating the single-particle gap. This speculation, however, can only be validated by a further quantitative theoretical analysis.

In conclusion, in a two-subband GaAs/AlGaAs two-dimensional electron system, a topological diagram of resistivity in density and magnetic field plane evolves from ring-like structures into a squarelike structures at higher magnetic fields. On each boundary of the square structure where spin split intersubband LLs are degenerate, an anticrossing gap was revealed by the thermally activated behavior. The simulation of the phase-diagram topology based on the DOS calculation of anticrossed intersubband LLs shows good qualitative agreement with the experiment. We attribute the origin of the gaps to pseudospin-ferromagnetism as reported before.

[1] See *Perspectives in Quantum Hall Effect*, edited by S. Das Sarma and A. Pinzuk (Wiley, New York, 1997), Chap. 5.

[2] T. Jungwirth and A. H. MacDonald, Phys. Rev. B **63**, 035305 (2001).

[3] T. Jungwirth, S. P. Shukla, L. Smrčka, M. Shayegan, and A. H. MacDonald, Phys. Rev. Lett. **81**, 2328 (1998).

[4] E. P. De Poortere, E. Tutuc, S. J. Papadakis, and M. Shayegan, Science **290**, 1546 (2000).

[5] V. Piazza, V. Pellegrini, F. Beltram, W. Wegschneider, T. Jungwirth, and A. H. MacDonald, Nature (London) **402**, 638 (1999).

[6] K. Lai, W. Pan, D. C. Tsui, S. Lyon, M. Mühlberger, and F. Schäffler, Phys. Rev. Lett. **96**, 076805 (2006).

[7] X. C. Zhang, D. R. Faulhaber, and H. W. Jiang, Phys. Rev. Lett. **95**, 216801 (2005).

[8] A. J. Daneshvar, C. J. B. Ford, M. Y. Simmons, A. V. Khaetskii, A. R. Hamilton, M. Pepper, and D. A. Ritchie, Phys. Rev. Lett. **79**, 4449 (1997).

[9] G. F. Giuliani and J. J. Quinn, Phys. Rev. B **31**, 6228 (1985); Surf. Sci. **170**, 316 (1986).

[10] K. Muraki, T. Saku, and Y. Hirayama, Phys. Rev. Lett. **87**, 196801 (2001).

[11] X. Y. Lee, H. W. Jiang, and W. J. Schaff, Phys. Rev. Lett. **83**, 3701 (1999).

[12] C. Ellenberger, B. Simovic, R. Leturcq, T. Ihn, S. E. Ulloa, K. Ensslin, D. C. Driscoll, and A. C. Gossard, cond-mat/0602271 (unpublished).